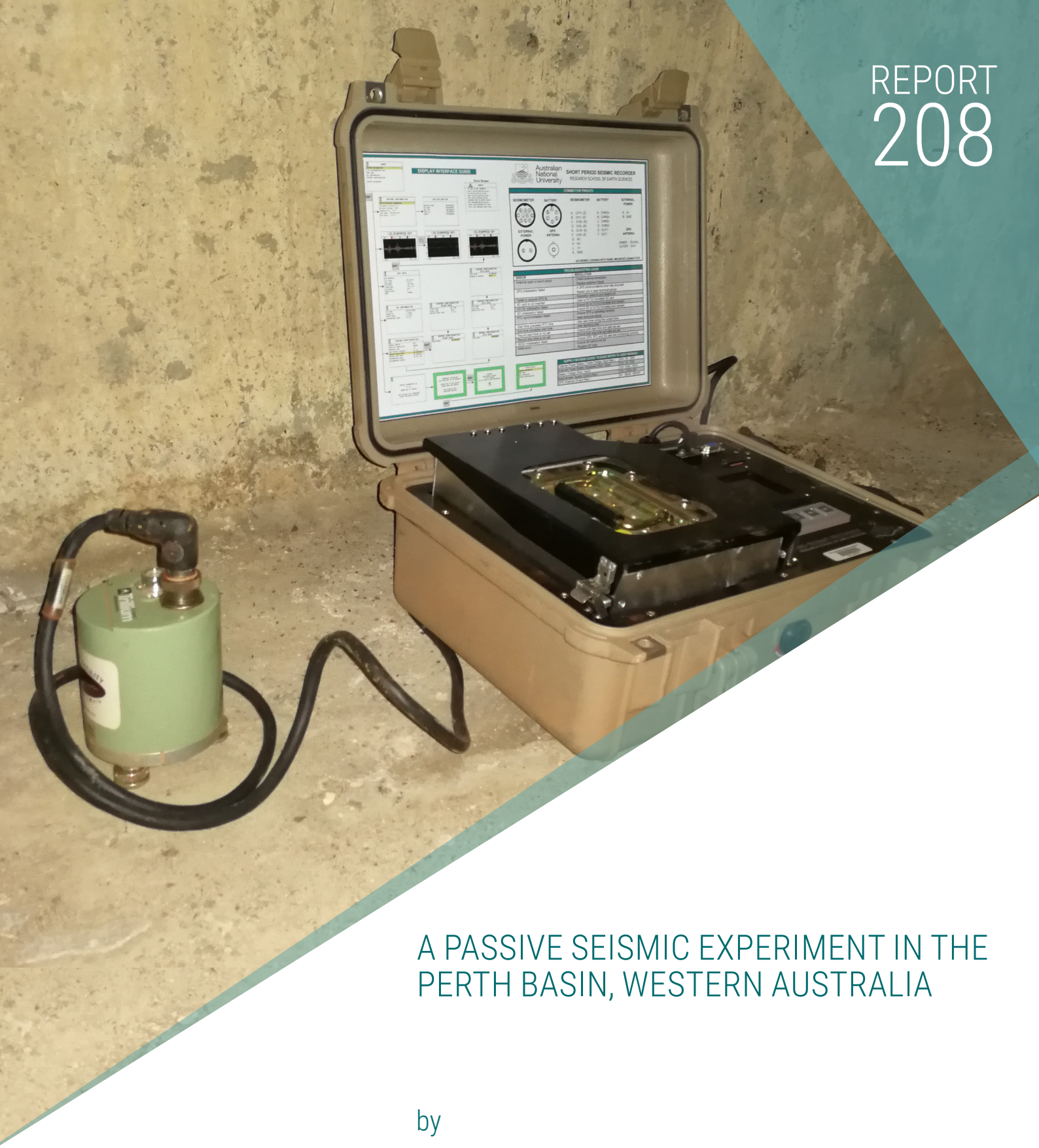

REPORT
208

A PASSIVE SEISMIC EXPERIMENT IN THE PERTH BASIN, WESTERN AUSTRALIA

by
RE Murdie, H Yuan, M Dentith and X Lin

EIS Exploration Incentive Scheme
The University of Western Australia
Centre for Exploration Targeting
Macquarie University
CCFS

Government of Western Australia
Department of Mines, Industry Regulation and Safety

Geological Survey of Western Australia

Government of **Western Australia**
Department of **Mines, Industry Regulation and Safety**

REPORT 208

A PASSIVE SEISMIC EXPERIMENT IN THE PERTH BASIN, WESTERN AUSTRALIA

by
RE Murdie, H Yuan[1,2], M Dentith[1] and X Lin[3]

1 Centre for Exploration Targeting, School of Earth Sciences,
The University of Western Australia, Stirling Highway, Crawley WA 6009, Australia
2 Macquarie University, Balaclava Road, North Ryde NSW 2109, Australia
3 Institute of Geology and Geophysics, Chinese Academy of Sciences, Beijing, China

PERTH 2020

Geological Survey of Western Australia

MINISTER FOR MINES AND PETROLEUM
Hon Bill Johnston MLA

DIRECTOR GENERAL, DEPARTMENT OF MINES, INDUSTRY REGULATION AND SAFETY
David Smith

EXECUTIVE DIRECTOR, GEOLOGICAL SURVEY AND RESOURCE STRATEGY
Jeff Haworth

REFERENCE
The recommended reference for this publication is:
Murdie, RE, Yuan, H, Dentith, M and Lin, X 2020, A passive seismic experiment in the Perth Basin, Western Australia: Geological Survey of Western Australia, Report 208, 19p.

ISBN 978-1-74168-901-3
ISSN 1834-2280

A catalogue record for this book is available from the National Library of Australia

Grid references in this publication refer to the Geocentric Datum of Australia 1994 (GDA94). Locations mentioned in the text are referenced using Map Grid Australia (MGA) coordinates, Zone 50. All locations are quoted to at least the nearest 100 m.

Published 2020 by the Geological Survey of Western Australia
This Report is published in digital format (PDF) and is available online at <www.dmirs.wa.gov.au/GSWApublications>.

Further details of geoscience publications are available from:
Information Centre
Department of Mines, Industry Regulation and Safety
100 Plain Street
EAST PERTH WESTERN AUSTRALIA 6004
Telephone: +61 8 9222 3459 Email: publications@dmirs.wa.gov.au
www.dmirs.wa.gov.au/GSWApublications

Cover photograph: A seismometer and recording instrumentation in the basement of Mineral House, Perth, Western Australia

Contents

Figures

Table

A passive seismic experiment in the Perth Basin, Western Australia

by

RE Murdie, H Yuan[1,2], M Dentith[1] and X Lin[3]

Abstract

To assess the feasibility of using passive seismic techniques in difficult environments, a passive seismic experiment was undertaken in the onshore Perth Basin. The Perth Basin is a long, thin geological basin next to a transcrustal fault scarp in an urban environment. Data was collected from an array of 29 stations. These stations comprised a north–south transect from near Moora in the north to near Harvey in the south, with a shorter east–west transect near Moora and extending on to the adjacent Yilgarn Craton. Additional data were also acquired in the Perth metropolitan area from 10 more installations. The project also aimed to image the Moho in an attempt to learn more about the mechanism of the creation of the Perth Basin.

Data analysis using common conversion point stacking of teleseismic arrivals and ambient noise tomographic methods allows crustal velocity structure to be mapped at a regional scale. In general, signal-to-noise levels were poor, largely due to shorter than expected deployment times. This resulted in poor resolution of the deep geology. Consequently, the Moho is only poorly constrained to be at a depth of more than about 45 km due to it being at the limit of data resolution. It is possibly represented by a velocity transition rather than a sharp discontinuity. The thickness of the Perth Basin, at around 10 km, is consistent with previous estimates based on interpretation of seismic reflection data. Beneath the basin, the crust has a largely consistent shear wave-velocity structure with laterally continuous zones. Shear velocities reach 4 km/s immediately below the Perth Basin within the basement rocks which are assumed to be part of the Pinjarra Orogen, typically extending to about 25 km depth. Beneath this is a layer of lower velocity, typically as low as 3.5 km/s which is particularly evident between 31.5°S and 32.3°S. Here, the different structure may be due to a different crustal component of the Pinjarra Orogen, perhaps reflecting the presence of a basement block with different affinities to elsewhere in the survey area.

KEYWORDS: ambient noise, Moho, passive seismic monitoring, Perth Basin, receiver functions

Introduction

A feasibility study for the use of passive seismic techniques within a long thin sedimentary basin has been completed in the onshore Perth Basin. Twenty-nine stations were deployed for six months along a north–south transect of the Perth Basin, including within the metropolitan area from Moora in the north to Harvey in the south (Figs 1, 2) and a shorter east–west transect near Moora, which extends on to the adjacent Yilgarn Craton. This was along a similar profile to two seismic lines; the New Norcia seismic line (NN92-01) shot in the early 1990s (Middleton et al., 1993) and BR71-AJ (a survey from 1971 shot with dynamite), and also covered by a magnetotelluric survey (Hoskin, 2017). Additional data were also acquired across the Perth metropolitan area which were also part of a parallel study to compare regular seismic monitoring with distributed acoustic sensing (DAS) which records motion sensed along fibre-optic cables (Shragge et al., 2019).

1 Centre for Exploration Targeting, School of Earth Sciences, The University of Western Australia, Stirling Highway, Crawley WA 6009, Australia
2 Macquarie University, Balaclava Road, North Ryde NSW 2109, Australia
3 Institute of Geology and Geophysics, Chinese Academy of Sciences, Beijing, China

The data were analysed using both teleseismic arrivals from distant earthquakes and also the background noise which is continuously recorded. Common conversion point (CCP) stacking of the receiver function of teleseismic arrivals and ambient noise tomographic methods allow crustal velocity structure to be mapped at the regional scale. This was a test case to see if it was possible to obtain useful data in an urban or semi-urban environment due to the noise levels. There was also concern that the shape of the Perth Basin, extremely long and thin with a potential vertical reflector (the Darling Fault) to one side, would be problematic.

Pre-Perth Basin geology

The Perth Basin lies to the west of the Archean Yilgarn Craton (Fig. 1). No Archean rocks have been reported to the west of the Darling Fault, a major structure that defines the eastern margin of the Perth Basin for much of its extent (>1000 km). The Darling Fault lies at the western edge of the Darling Fault Zone, an approximately 10 km-wide zone that records brittle and ductile deformation along the western margin of the Yilgarn Craton with a long history of varying styles of deformation dating back to at least the Proterozoic (Harris, 1994; Crostella and Backhouse, 2000). Forward gravity modelling (Iasky, 1993; Holzrichter et al., 2014) suggests that the Darling Fault is a planar, crustal-scale structure that offsets the Moho.

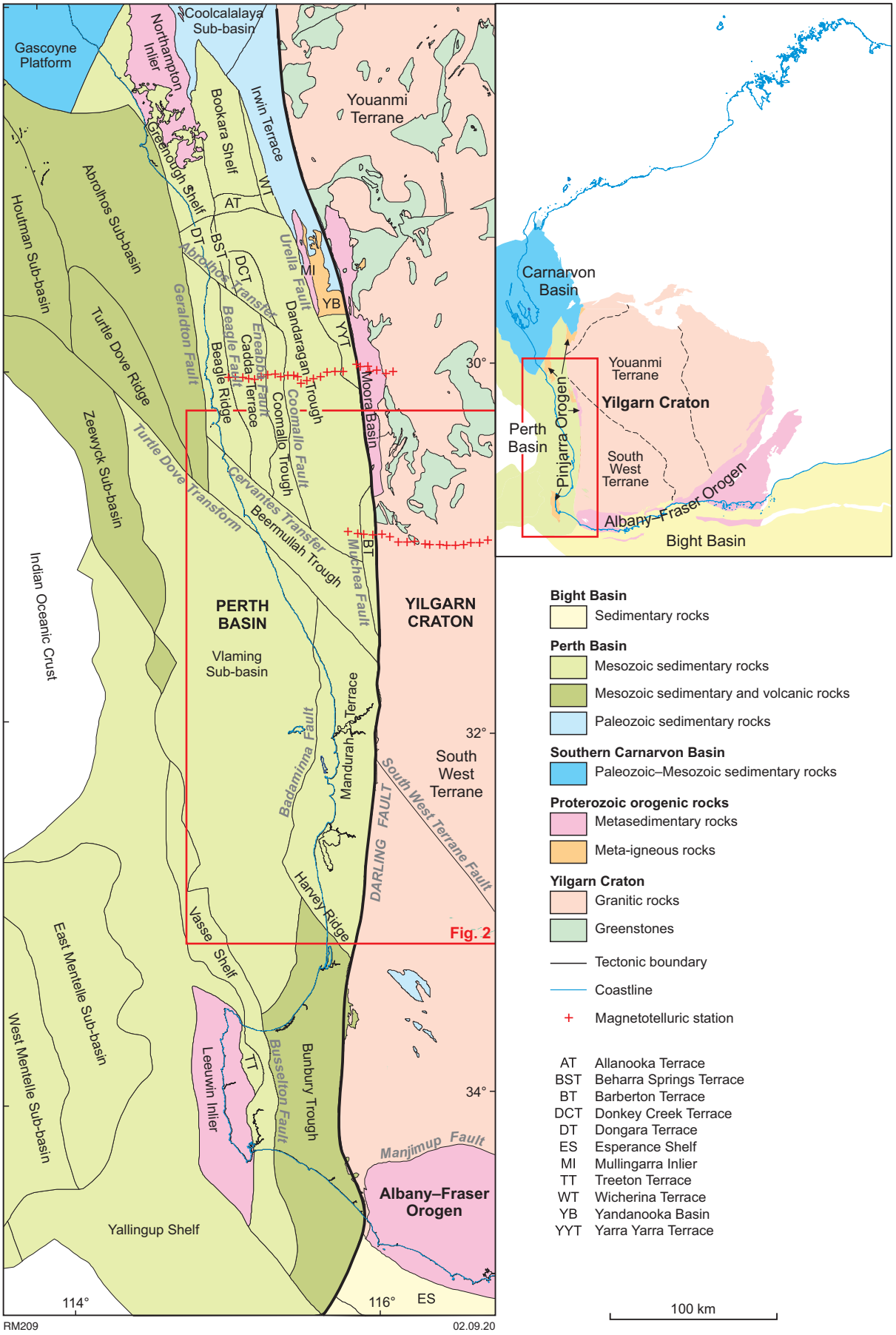

Figure 1. Tectonic components of the Perth Basin and adjacent geology of the Yilgarn Craton

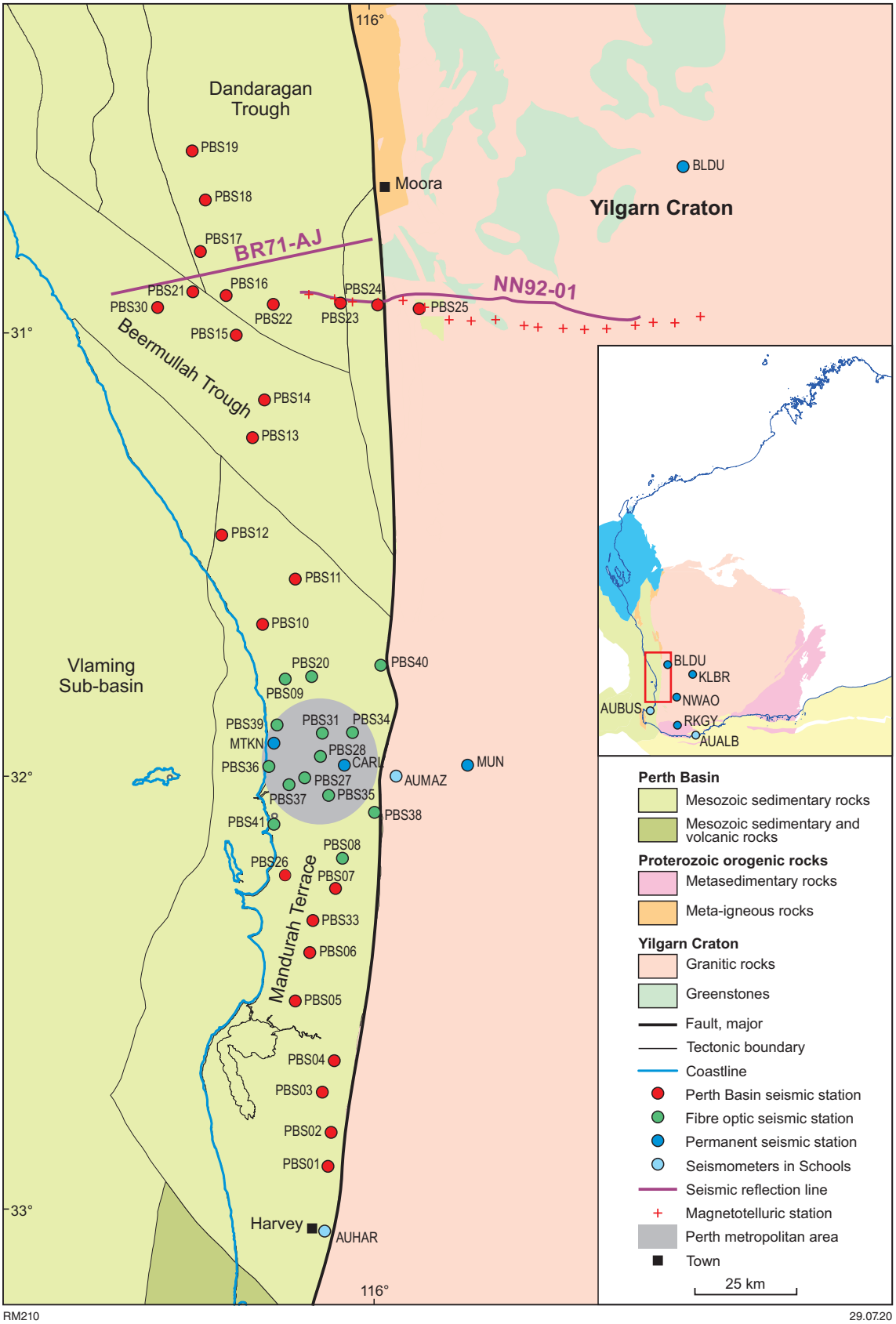

Figure 2. Location of the passive seismic network in relation to the tectonic components of the Perth Basin (see Fig. 1)

There are many unresolved questions about the timing of Phanerozoic movement on the Darling Fault. Throw along the Darling Fault varies greatly, and it remains unclear if it has always been the long, continuous structure it is today.

Mostly to the west of the Darling Fault, but also extending across to adjacent areas of the Yilgarn Craton, are the rocks comprising the Pinjarra Orogen. The Pinjarra Orogen is spatially near coincident with the onshore Perth Basin. However, comparatively little is known about the orogen since most of it exists beneath a thick cover of Perth Basin sediments. There have been some intersections of igneous and metamorphic basement rocks in wells or drillholes in the Perth Basin (Fletcher and Libby, 1993; Markwitz et al., 2017) and crystalline basement rocks outcrop in a series of inliers. The adjacent Proterozoic Northampton and Mullingarra complexes and the Neoproterozoic Leeuwin complex (Wilde, 1999), are interpreted as a series of distinct terranes assembled during multiple orogenic events in the Proterozoic (Janssen et al., 2003; Johnson, 2013). Thus, the basement to the Perth Basin probably comprises a collage of suspect terranes, and by implication, there is likely to be distinctly different basement geology in different areas. However, without appropriate geophysical data, this geological scenario is untested (Iasky and Lockwood, 2004; Hall et al., 2012).

Geology of the Perth Basin

History

There is limited outcrop of Perth Basin strata south of the Perth metropolitan area (Lowry, 1965), and what is exposed mostly comprises Cenozoic rocks and unconsolidated sediments. Therefore, much of the stratigraphy and structure of this part of the Perth Basin has been established from drilling and geophysical data. However, geophysical and borehole data in the Perth Basin have uneven distribution and depth of penetration, so many of the components of the basin fill are only poorly defined and understood (Delle Piane et al., 2013). The regional seismic interpretation of Mory and Iasky (1996) determined the broad structural architecture of both the onshore and part of the offshore southern Perth Basin. Olierook et al. (2015) built a 3D model to look at the potential for hydrocarbon and geothermal prospects, and effective aquifer management.

Various tectonostratigraphic schemes and basin tectonic phases have been proposed for the Perth Basin (summarized in Thomas, 2014). The Perth Basin initially formed as part of the East Gondwana interior rift–sag system. The southern Perth Basin was situated in a more interior position of the East Gondwana rift compared to the northern Perth Basin and the Carnarvon Basin (Haig et al., 2014), which was more proximal to the then continental–oceanic crust boundary. This meant that the marine incursions that deposited the latest Permian – Early Triassic in the northern Perth Basin did not reach the southern Perth Basin, and a continental depositional environment was maintained throughout its entire evolution until continental breakup.

The oldest recorded sedimentary rocks occur in the north of the Perth Basin and belong to the Tumblagooda Sandstone of probable Ordovician to earliest Silurian age (Hocking, 1991; Mory and Hocking, 2008).

Across the entire onshore basin, a middle Carboniferous to middle Permian succession records a period of glaciation and subsequent deglaciation in a marine-influenced depositional setting in the north and a continental setting in the south (Cockbain and Lehmann, 1971; Quaife et al., 1994; Crostella and Backhouse, 2000). At the top of this succession is a middle Permian unconformity (Cockbain and Lehmann, 1971; Quaife et al., 1994). The overlying upper Permian unit is marine in the north and fluvial in the south (Mory and Iasky, 1996; Crostella and Backhouse, 2000). The Triassic to pre-breakup Cretaceous units record mainly fluvial to lacustrine deposition punctuated by briefer episodes of shallow-marine deposition continuing until continental breakup (Cockbain and Lehmann, 1971; Playford et al., 1976; Crostella and Backhouse, 2000). The majority of deposition occurred during the late Triassic to Cretaceous during continental breakup (Playford et al., 1975).

The syn-rift succession in the Permian is the result of southwest–northeast extension (e.g. Harris, 1994; Tupper et al., 1994; Mory and Iasky, 1996; Song and Cawood, 2000; Norvick, 2004; Jones et al., 2011). There is another phase of rifting in the lower Jurassic although the timing and direction of extension is variously interpreted (Thomas, 2014).

The Upper Jurassic and the lowermost Cretaceous strata are syn-rift successions laid down in response to northwest–southeast rifting during the breakup and separation of Greater India from the Australian–Antarctic continent to form the Indian Ocean (Iasky, 1993; Harris, 1994; Song and Cawood, 2000; Nicholson et al., 2008; Jones et al., 2011; Gibbons et al., 2012). The breakup unconformity sits either just below or within a succession of rift-related basalt extrusions (collectively known as the Bunbury Basalt) that range in age from c. 137 to 130 Ma (Olierook et al., 2016).

Structure

The broad architecture of the Perth Basin was initially revealed by a regional-scale gravity survey (Thyer and Everingham, 1956). This showed that the onshore basin comprises two north–south trending, westwards-shallowing depocentres west of the Darling Fault, which they named the Dandaragan and Bunbury Troughs (Fig. 1). Subsequent offshore seismic, gravity and magnetic surveys have allowed additional major depocentres to be delineated, namely the Abrolhos, Houtman and Vlaming Sub-basins (Playford, 1971; Jones and Pearson, 1972; Symonds and Cameron, 1977).

In the onshore basin, a series of north to north-northwesterly trending normal faults (F_1) have been mapped, and are interrupted by what have been interpreted as east–west (F_2), northeast (F_3)- and northwest (F_4)-striking transfer (strike-slip) faults reflecting underlying basement shear zones (e.g. Byrne and Harris, 1992; Dentith et al., 1994; Harris, 1994), and/or contrasts in basement rheology (Dentith et al., 1994).

The F_1 north-northwesterly striking lineaments dominate the geometry and depocentres of the Perth Basin and generally exhibit normal movement with some reverse and dextral strike-slip components due to reactivation. These faults were activated during the rifting phases. Variations in extensional orientation lead to the development of local compressional deformation (Iasky and Shevchenko, 1996; Mory and Iasky, 1996; Thomas, 2014).

The F_2 faults acted as linkage features between the various north-trending faults. They were initiated as strike-slip faults in the Jurassic extension (Harris, 1994; Song and Cawood, 2000). Local basin inversion occurred due to localized compression at fault bends in the middle Jurassic to early Cretaceous (Song and Cawood, 2000). F_3 lineaments seen in the gravity and aeromagnetic data appear to offset F_1 faults with dextral movement and are interpreted to be en echelon segments of the F_1 faults. F_4 faults are interpreted as transfer faults/zones.

The major components of the Perth Basin within the area of the passive seismic study are described below and illustrated in Figures 1 and 2.

Dandaragan Trough

The north–south trending Dandaragan Trough (Thyer and Everingham, 1956) is a half-graben with up to 12 km of Permian and younger strata (Mory and Iasky, 1996), and is the deepest onshore depocentre of the Perth Basin. Green and Duddy (2013) suggested there has been little uplift and exhumation of the Dandaragan Trough. It is associated with a marked gravity low interpreted to be due to a deeper Moho under the basin (Holzrichter et al., 2014).

The Dandaragan Trough is bounded by the Darling and Muchea Faults to the east, the Eneabba Fault System to the west (Crostella, 1995; Mory and Iasky, 1996), and the Cervantes Transfer Fault as the southern boundary with the Beermullah Trough (Crostella and Backhouse, 2000).

Darling, Muchea and Urella Faults (Darling Fault Zone)

The Darling, Muchea and Urella Faults are the main faults at or near the eastern margin of the Perth Basin. They were the primary control over sedimentation in the north Perth Basin (Mory and Iasky, 1996).

Harvey Ridge

The Harvey Ridge is a roughly east–west to southeast–northwest-oriented structural high seen in seismic sections and is associated with a higher gravity anomaly than adjacent areas (Sealy, 1969). Located between the Bunbury Trough and Mandurah Terrace, it is a broadly northwesterly trending anticline that began to form during the Late Jurassic – Early Cretaceous (Thomas, 2018).

Mandurah Terrace

The Mandurah Terrace is a half-graben bounded to the west by the Badaminna Fault System and to the east by the Darling Fault. It separates the main depocentres of the Dandaragan Trough to the north and the Bunbury Trough to the south. Pre-breakup (Permian – Early Cretaceous) strata generally become deeper with age towards the north, and are shallowest in the south where they were uplifted to form the Harvey Ridge.

Vlaming Sub-basin

The mostly offshore Vlaming Sub-basin (Jones and Pearson, 1972) lies west of the Mandurah Terrace, and is separated from it by the westerly dipping Badaminna Fault System. The Vlaming Sub-basin has more than 12 km of sedimentary fill (Nicholson et al., 2008). The sub-basin is interpreted to have been a major depocentre during Jurassic times (Nicholson et al., 2008).

Economic significance of the Perth Basin

Petroleum exploration in the Perth Basin started in the early 1950s and since then over 368 onshore and 61 offshore wells have been drilled. Several commercial oil and gas fields have been discovered and developed, making it the second largest petroleum producer after the Northern Carnarvon Basin within Western Australian jurisdiction. All producing fields are located within the northern Perth Basin, where oil and gas has been produced from several onshore fields and oil from one offshore field.

Besides conventional petroleum resources, resource estimates indicate tight sand / shale gas and oil up to 25 trillion cubic feet (Tcf) gas in the Permian Carynginia Formation, and within the latest Permian–Triassic Kockatea Shale, up to 8 Tcf gas with 500 million barrels of oil/condensate (Kuuskraa et al., 2011, 2013).

The area around Harvey has been explored with deep drillholes (Millar and Reeve, 2014) and seismic lines (Zhan, 2014) to investigate its potential for geosequestration of CO_2 in a project sponsored by the Carbon Storage Taskforce established by the Australian Government.

Aquifers in the Perth Basin have also been identified as having suitable conditions for production of geothermal energy. Several shallow (2.0 – 3.5 km), low temperature (65–80°C) projects have been using groundwater for heating swimming pools and buildings since 1997 (Pujol et al., 2015) with more commercial schemes coming online in 2016. There are mid-temperature (80–140°C) hot sedimentary aquifer resources inferred to be present in the central and northern Perth Basin (Middleton, 2016). However, significant gaps in the geological understanding of the Perth Basin are preventing these from being known (and proven) resources (Timms et al., 2012).

Seismic data acquisition

Passive seismic monitoring was carried out in the Perth Basin from January to June 2017. Twenty-nine seismometers were deployed comprising a north–south array extending from near Moora to near Harvey with a secondary shorter perpendicular array at the latitude of

Moora (Fig. 2). The Moora east–west line was located to coincide with an existing magnetotelluric line (Hoskin, 2017) which also lies close to a deep seismic reflection line (NN92-01, Dentith et al., 1993), one of the few seismic lines to cross the basin edge on to the adjacent Yilgarn Craton. Petroleum exploration line BR71-AJ is on the basinside continuation of NN92-01.

Passive seismic stations were spaced about 12 km apart. Stations were deployed for approximately six months, although problems maintaining power supply meant that data recording was rarely continuous over the entire deployment period. To maximize spatial coverage, which is especially important for ambient noise tomography, the overall deployment was designed to link with currently deployed seismic stations in the area operated by Geoscience Australia (GA), the station at Mount Kenneth Jump (MKTN) in the Perth region, the Mundaring station (MUN) and Carlisle Jump (CARL; Fig. 2). Stations from the Seismometers in Schools program were also used, including those from: Mazenod Senior College (AUMAZ), St Anne's School in Harvey (AUHAR), St Joseph's College in Albany (AUALB) and Georgiana Molly Anglican School in Busselton (AUBUS). Regional permanent stations operated by GA are located in Narrogin (NWAO), Rocky Gully (RKGY), Ballidu (BLDU), and Kellerberrin (KLBR).

In addition to the two traverses, extra stations were deployed in the Perth metropolitan area from March to November 2017 as part of another study involving the use of a fibre-optic cable as a seismic receiver (Shragge et al., 2019). A total of 39 stations was deployed across these two projects.

Sensors used for the two traverses were mainly Nanometrics Trillium broadband seismometers with optimum response range from 20 s to 100 Hz. These instruments were on loan from the Australian National Seismic Imaging Resource (ANSIR). The seismometers used in the metropolitan areas were also Nanometrics Trillium broadband seismometers, but with a wider spectrum of 120 s to 100 Hz. These instruments were part of The University of Western Australia – Australian National University – University of Melbourne (WAM) pool. The instruments deployed in the south were deployed on the surface, mostly within buildings, whereas the deployments in the north were mostly buried to a depth of a few tens of centimetres. The subsurface sensors produced less noisy data.

All data were recorded on Australian National University-designed digital acquisition systems. Each digitizer was internally powered by its own battery. The specifications of the digital acquisition system indicated that the battery could power the site for three months, although this was rarely the case and hence there were many discontinuities in the data. All data were recorded at 200 Hz and down sampled where necessary.

Seismic data processing

From 24 January to 30 November 2017, approximately 600 earthquakes of magnitude (M) greater than five occurred within 80° of the Perth Basin array (Fig. 3). These events tend to originate from the Indonesian and Japanese arcs and New Zealand, heavily biasing events to the north-northeast clockwise through to the southeast. The southwest quadrant was poorly represented; however, during this time there were a few events along the Central Indian Ridge and Southeast Indian Ridge that could be used.

Receiver function analysis

Receiver functions (Ammon, 1991) use arrivals from teleseismic events to locate major velocity discontinuities within the crust. Figure 4 is an example of a teleseismic recording showing vertical-component waveforms for an M6.9 earthquake that occurred in Tonga. The P-wave arrival at each station is marked with a tick. Waveforms are high-pass filtered with the lower corner frequency at 0.3 Hz. Major velocity discontinuities are mapped because they are locations where mode conversion from P- to S-waves can occur during the transmission or reflection of the seismic waves (Fig. 5). The relative travel times and amplitudes of arrivals of the different phases, as represented in the receiver function, form the basis for deriving crustal velocity variations.

The travel paths of all earthquakes at all stations were back projected along their incident pathway (Fig. 6) according to their origin. The energy from each segment of the travel path is separated out into bins within a seismic velocity model following the method of Dueker and Sheehan (1997). The seismic model volume that was created is 300 × 150 km at the surface and 100 km deep, and divided into bins of 2 × 2 km wide at the surface and 1 km in thickness. The receiver function energy from all earthquakes in each bin uses CCP stacking. A peak period of 2 s is used to calculate the region influencing each receiver function path, which is approximated by the first Fresnel zone $\sqrt{(0.5\lambda z_i)}$, where λ is the wavelength and z_i is the depth of the bin. Hence, longer wavelengths affect a wider area and overlap with other events, so the image created by CCP stacking becomes smoothed at depth.

Bootstrapping (Efron and Tibshitani, 1986) was used to average the energy within each model bin. A continuous velocity map in 3D is obtained with the Moho and other intracrustal and intramantle discontinuities showing as velocity gradients. The bootstrapping procedure also returns the standard deviation of receiver function energy, which is approximated as the CCP stacking error. The CCP data were compiled along four profiles; two north–south lines, an east–west line across the northern stations and a northeast–southwest line over the southern region of the study area (Figs 7, 8).

Ambient noise tomography

Large-scale shear wave-velocity variations were mapped using the ambient noise correlation technique (Shapiro and Campillo, 2004; Bensen et al., 2007; Saygin and Kennett, 2010, 2012). The product is a seismic velocity model of the crust and upper mantle (Shapiro and Campillo, 2004). The advantage of using ambient noise is that it comprises diffusive energy in random directions and it is not necessary to wait for an earthquake to occur. For crustal-scale studies, the diffusive energy sources are usually from the ocean wave noise along the coastline. This technique is best for imaging broad regions of different seismic properties, but not for imaging discontinuities, and hence is complementary to the CCP method.

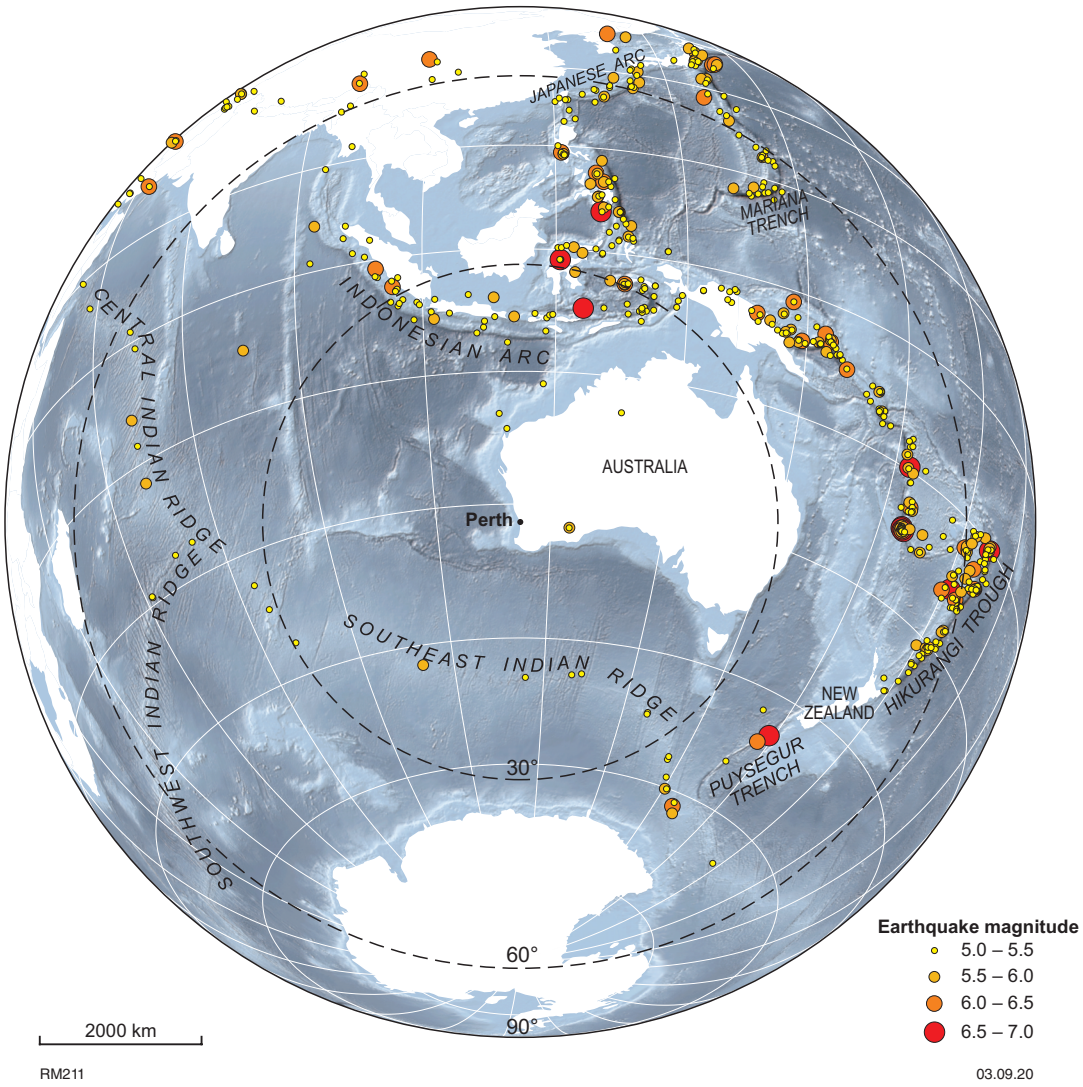

Figure 3. Earthquakes M >5 and epicentral distance from 20 to 90° (dashed circle) from the Perth Basin array between 24 January and 30 November 2017. A total of ~240 teleseismic events was selected for receiver function analysis

The ambient noise method uses the dispersion of the Raleigh surface waves between two stations recording simultaneously and incorporates only the vertical component of the waveform (Fig. 9a). A cross-correlated signal is not symmetrical in energy (Fig. 9b), which shows that the distribution of the random diffusive energy sources is in general not directionally symmetrical. The original signals were down sampled to 10 Hz, and the amplitude normalized, demeaned and detrended. Cross-correlation used a 600 s time window to extract the Greens function from which the wave speeds can be derived. Using a short time window has the advantage that coherent dispersion signals are usually in phase and therefore can be stacked up, while random noise is stacked down (Fig. 9c). For each station, a bootstrap resampling (Efron and Tibshitani, 1986) was used to generate 100 sets of data which were then stacked and averaged. The bootstrapping of a large number of traces (~9000 per station pair) also enhances the signal-to-noise ratio and removes the effect of earthquakes and the uneven distribution of temporal noise sources.

The correlated traces were then band-pass filtered at different band widths from 2 to 30 s (Fig. 9d), which correspond to different depths of investigation, from near the surface to close to the Moho. Since surface waves are dispersive, the group and phase velocity can be measured for each frequency. Figure 9e demonstrates the dispersive nature of the cross-correlated waveform with the long periods arriving before the shorter periods. For this study, the group velocity was determined using the automated frequency time analysis code (Levshin et al., 1972).

The group velocities are measured between all station pairs that were active at the same time (Fig. 9f). Permanent stations and those in schools were also included so as to get sufficient path length to investigate Moho depths. The group velocities between pairs of stations at a particular frequency can be framed as a 2D tomographic problem, and a map of group velocity distribution is derived by the inversion of frequency/depth using a fast-marching surface wave tomography package (Rawlinson and Sambridge, 2005).

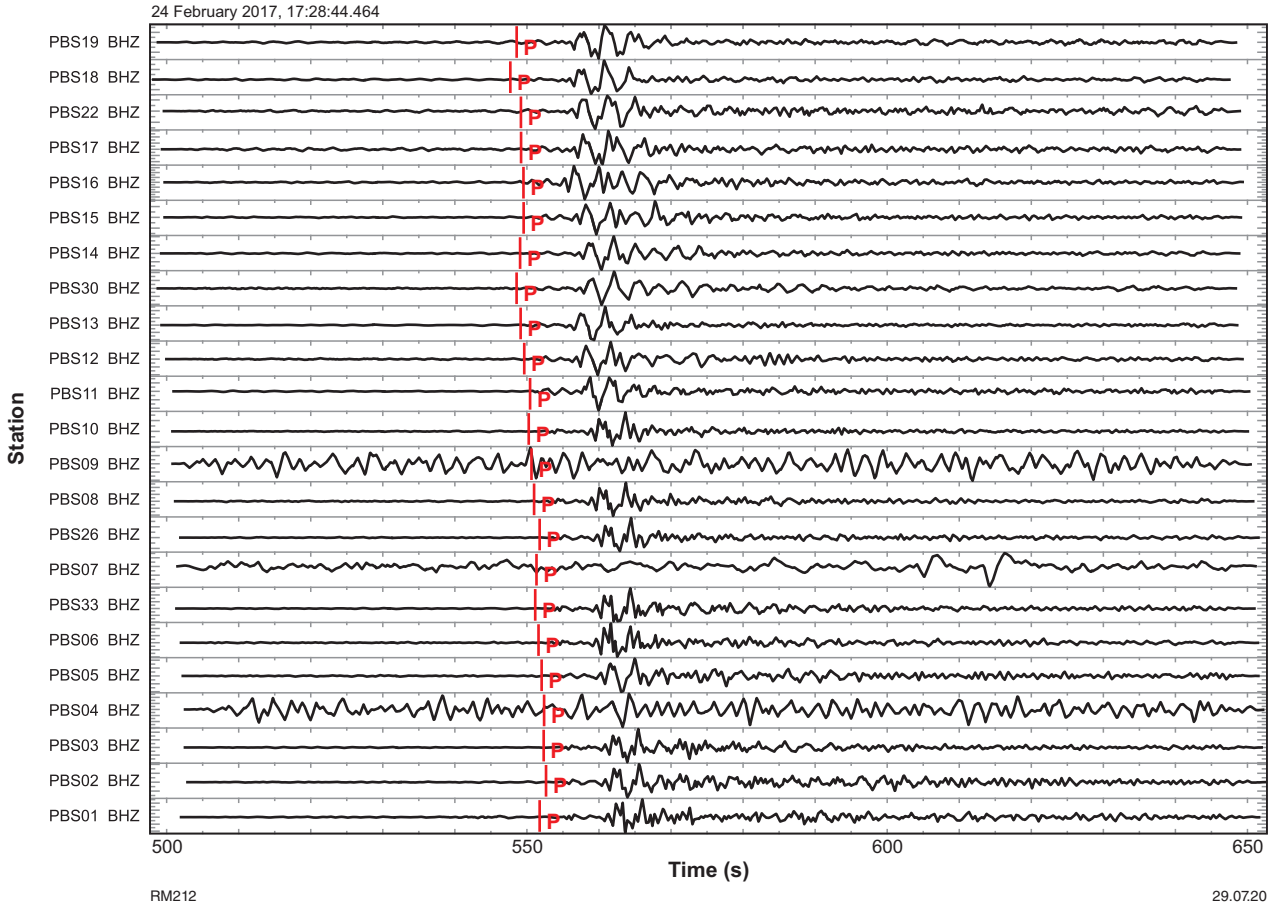

Figure 4. **The vertical-component waveforms for an Mw6.9 earthquake that occurred in Tonga. The P-wave arrival at each station is marked with a red line. Waveforms are high-pass filtered with the lower corner frequency at 0.3 Hz**

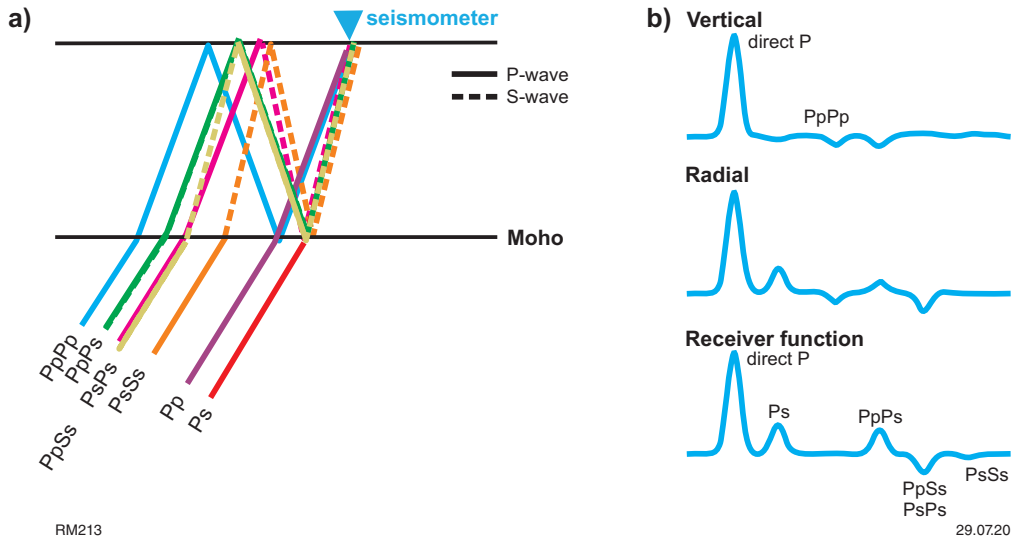

Figure 5. **Diagrammatic representation of the possible propagation modes through the Moho of an incoming P-wave: a) mode conversions of the incoming P-wave to either P- or S-waves in the crust with subsequent reflections at the Moho and free surface; b) the resulting receiver function**

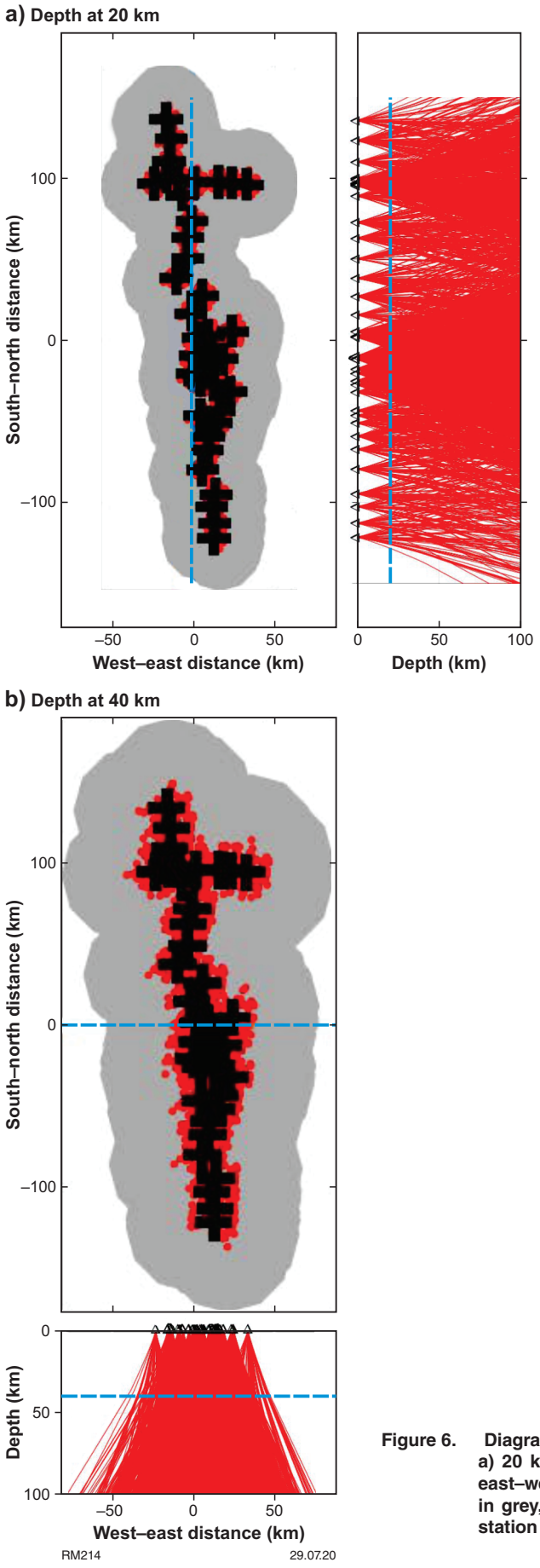

Figure 6. **Diagram of the raypaths used in the receiver function CCP analysis at: a) 20 km depth with vertical north–south profile; b) 40 km depth with east–west profile. The area of influence of ray paths at that depth is shown in grey, which is a function of the Fresnel zone. Black crosses are the station locations**

Yuan and Bodin (2018) provide a detailed description of the processing procedure. For each period, we used a 0.2 × 0.2° grid cell for the surface region that extends from –35.2 to –28.8° latitude and 115.2 to 118.0° longitude.

After the dispersion map inversion, for each 0.2 × 0.2° cell across the study area, a 1D shear wave profile was extracted using a modified transdimensional inversion approach (Yuan and Bodin, 2018) that incorporated a smooth background shear wave velocity (Vs) and the Moho topography from the Australian Seismological Reference Model (AuSREM; Salmon et al., 2012). The transdimensional inversion treats the number of vertical layers as a free parameter, which is determined on the fly by the inversion. Since this technique is sensitive only to the vertically polarized Vs (Vsv), the compressional velocity (Vp) and density are scaled using a Vp/Vs ratio of 1.75 and an empirical Vp to density relation. These 1D profiles are combined and interpolated to give a 3D volume of shear wave variation.

The longest wavelength processed was 25 s with a 10 s sensitivity kernel. This means that the deepest level in the model with reliable data is at about 30 km, but the tail off in sensitivity allows us to image (with larger errors) down to about 50 km. Reliability plots are given for each velocity model (Fig. 10b,d,f,h).

Profiles were extracted from the Vs model along two north–south lines (NS1 and NS2; Figs 7, 10a,c), one closer to the coast than the other, but both lying in regions of greatest station density within the Perth Basin. In addition, sections across the regional strike were extracted. The northernmost section (EW1, Fig. 10e) coincides with the east–west traverse near Moora. The southern section (EW2, Fig. 10g) trends northeast–southwest and takes advantage of the greater station density south of the Perth metropolitan area.

Seismic results

Perth Basin thickness

The thickness of the Perth Basin sedimentary sequence is best interpreted from the ambient noise plots (Fig. 10). A distinct low-velocity zone is well constrained by the ambient noise data, typically extending to about 10 km depth. There is an equivalent positive velocity gradient in the CCP (Fig. 8), albeit at a slightly shallower depth. North of latitude 31.5°S, the CCP signal becomes much less coherent especially on profile NS2, which is the approximate location where the Turtle Dove Ridge crosses the Perth Basin. However, this has no equivalent in the ambient noise model.

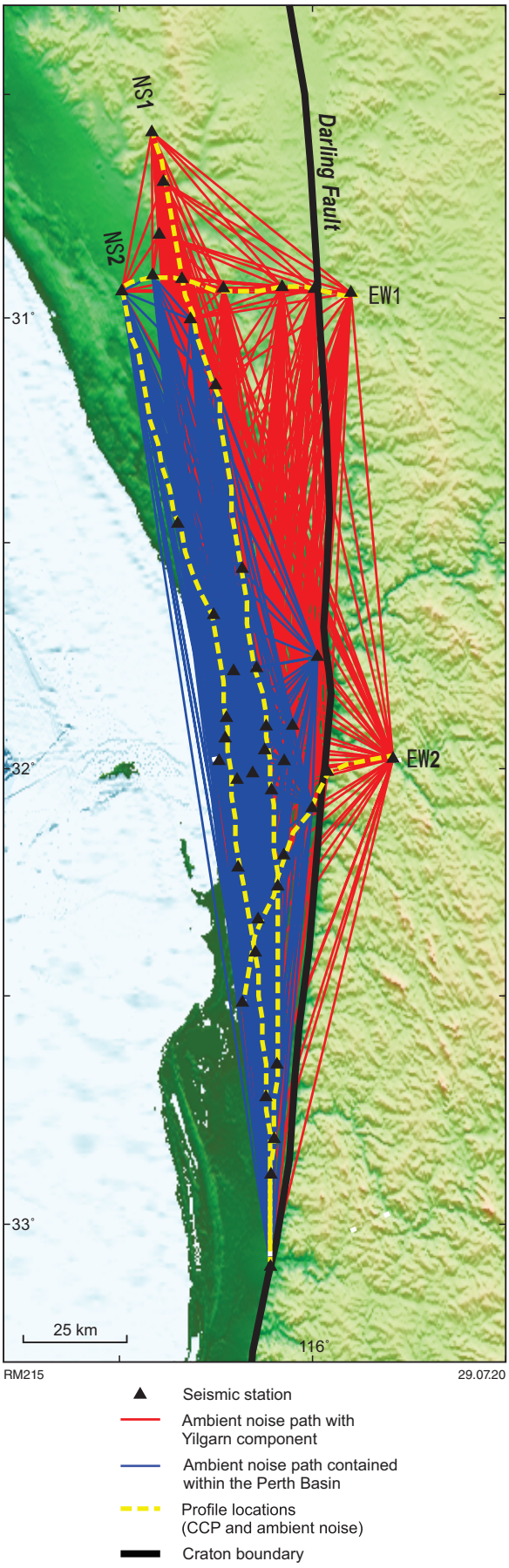

Figure 7. Location of extracted profiles from the ambient noise and CCP processing (yellow dashed lines) with an underlay of ambient noise ray paths. Blue ray paths are totally within the Perth Basin. Red ray paths sample a component of the Yilgarn Craton

In general, the depth of the low-velocity zone in the ambient noise model is consistent with the estimated basin depth from Mory and Iasky (1996). However, an apparent thinning of the basin to approximately 6 km in the south in the ambient noise model has no equivalent feature in the seismic reflection data. It is possible that it is an effect of the proximity and dip of the Darling Fault cutting the profile at depth.

The eastern edge of the Perth Basin is seen in the east–west profile EW1 as an abrupt edge in the CCP image and as a thinning of the low-velocity layer in the ambient noise model. This thinning probably represents a smoothing of the data across the transition from basin to craton. A slight thinning is seen in EW2.

Basement and middle to lower crust

The ambient noise model suggests a two-layered crustal structure under the Perth Basin in most of the profiles. At the southern end of the NS profiles, the crust that is sampled is from the Yilgarn Craton and shows different characteristics. Immediately underlying the low-velocity zone inferred to represent the Perth Basin sediments, is a laterally continuous zone with shear velocities that reach 4 km/s, typically extending to about 20 km depth. Beneath this is a laterally continuous, lower velocity layer, with velocities as low as 3.5 km/s.

The expected velocity gradients at the upper and lower edges of these layers are not well imaged in the CCP data, which typically show a negative gradient immediately beneath the large positive gradient associated with the base of the Perth Basin, but this is shallower than the change to low velocity seen in the ambient noise model.

In the lower crust, the CCP data show a negative gradient at 32.5°S, but this negative gradient is not evident elsewhere. This negative gradient does coincide with a change in velocity structure in the ambient noise profile, which, south of 32.5°S, shows a second low-velocity zone at depths of 10–20 km. This is probably a result of the profiles crossing the Darling Fault Zone, albeit at a highly oblique angle and thus the change in structure reflects the different velocity structure of the Yilgarn Craton.

An interesting feature in the ambient noise model is a low-velocity region seen in the lower crust between 31.5 and 32.3°S at depths of 20–30 km. It is possible that this represents a different crustal zone to the north, that is, a different crustal component of the Pinjarra Orogen.

Moho

Interpretations of the Moho depth have to be treated with caution due to the limitations of the frequencies used in the ambient noise processing technique. The results are only reliable down to 30 km depth, although the images produced show features down to 50 km. Features at depths between 30 and 50 km have been interpreted but with more caution than shallower features.

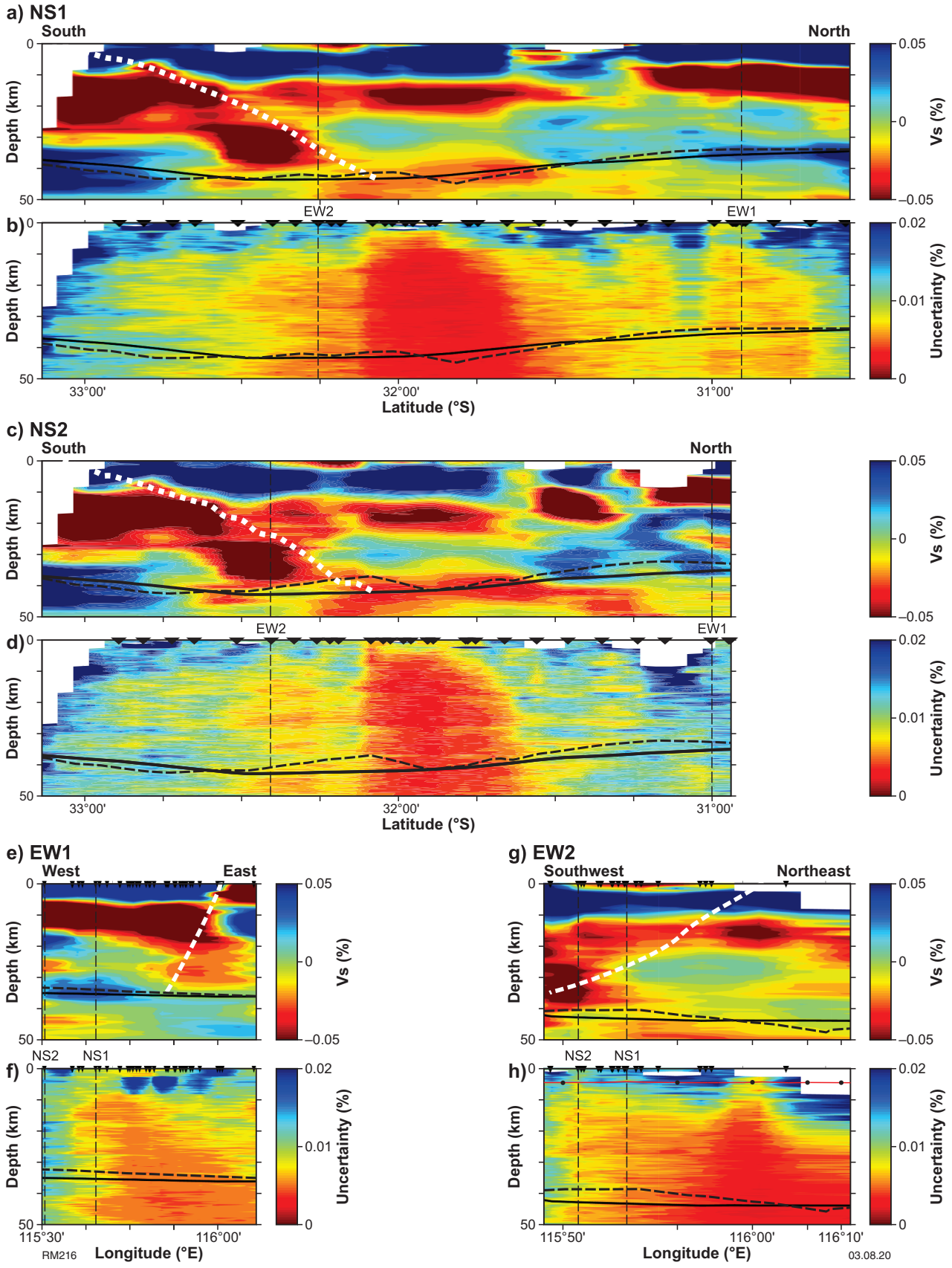

Figure 8. **CCP profiles for the Perth Basin transects: a, c, e, g) CCP profiles two north–south and two east–west. The depth of the Moho estimated using the AuSREM model is represented by the solid black line, and the dashed black line represents the MoGGIE Moho. The white dashed line shows the approximate position of the Darling Fault Zone; b, d, f, h) error percentage estimates for the associated CCP profile. Note the axis for EW2 is by longitude, but since the profile is oriented northeast–southwest, the scale does not represent true distance. The location of all of the profiles can be found in Figure 7**

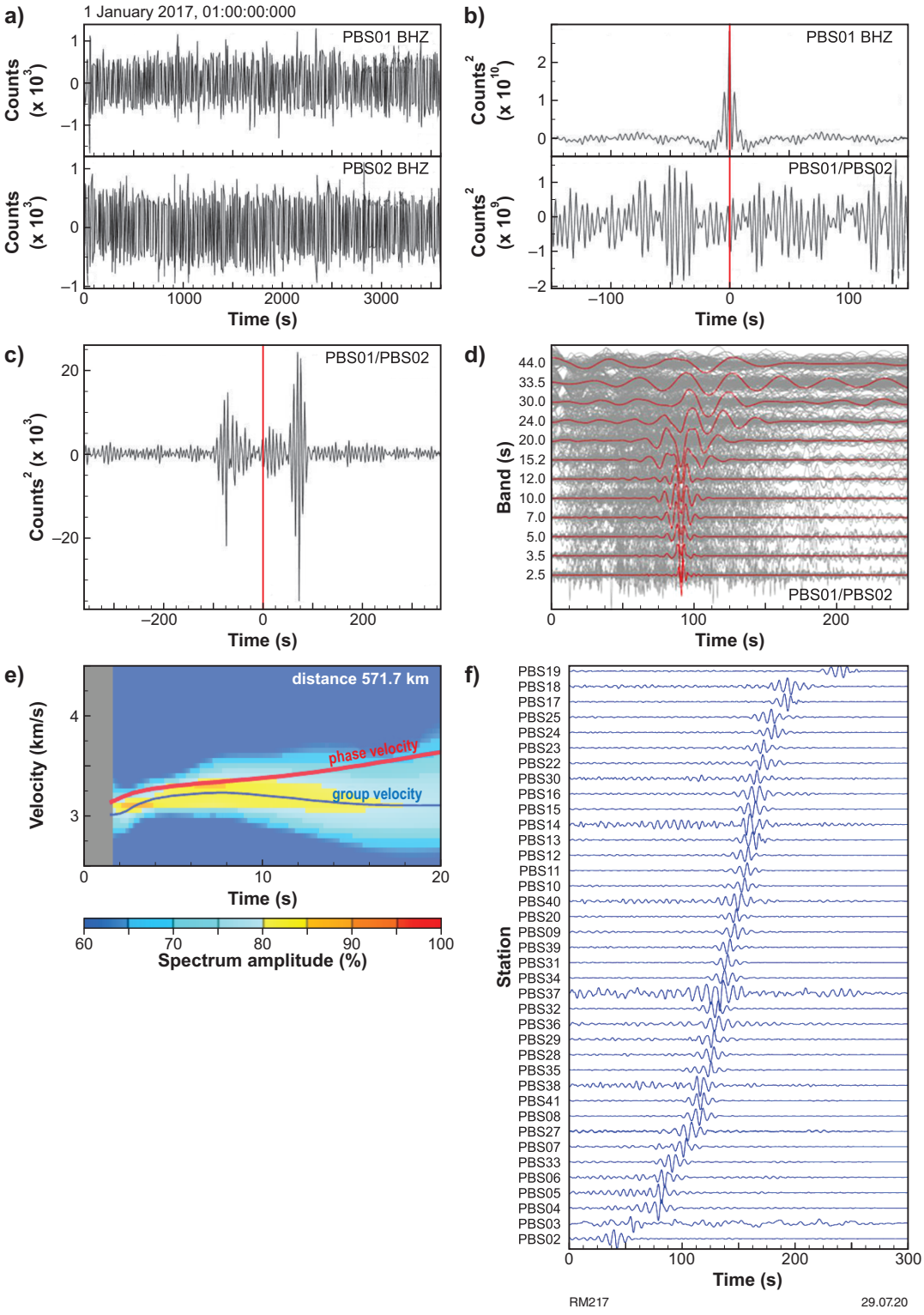

Figure 9. **Ambient noise processing: a) 10 minute-recording of noise at two stations, PBS01 and PBS02; b) auto- and cross-correlation of the signals from a); c) stacked cross-correlated signals over the duration of the data; d) stacked cross-correlated waveform (red) from one station pair, showing different frequency content. Grey traces are the unstacked waveforms over one month of 60-minute stacks at that frequency band; e) dispersion curves from cross-correlated waveforms of a station pair; f) an example of a stack of cross-correlated waveforms for station pairs formed by station PBS01 with all others, sorted by distance between stations**

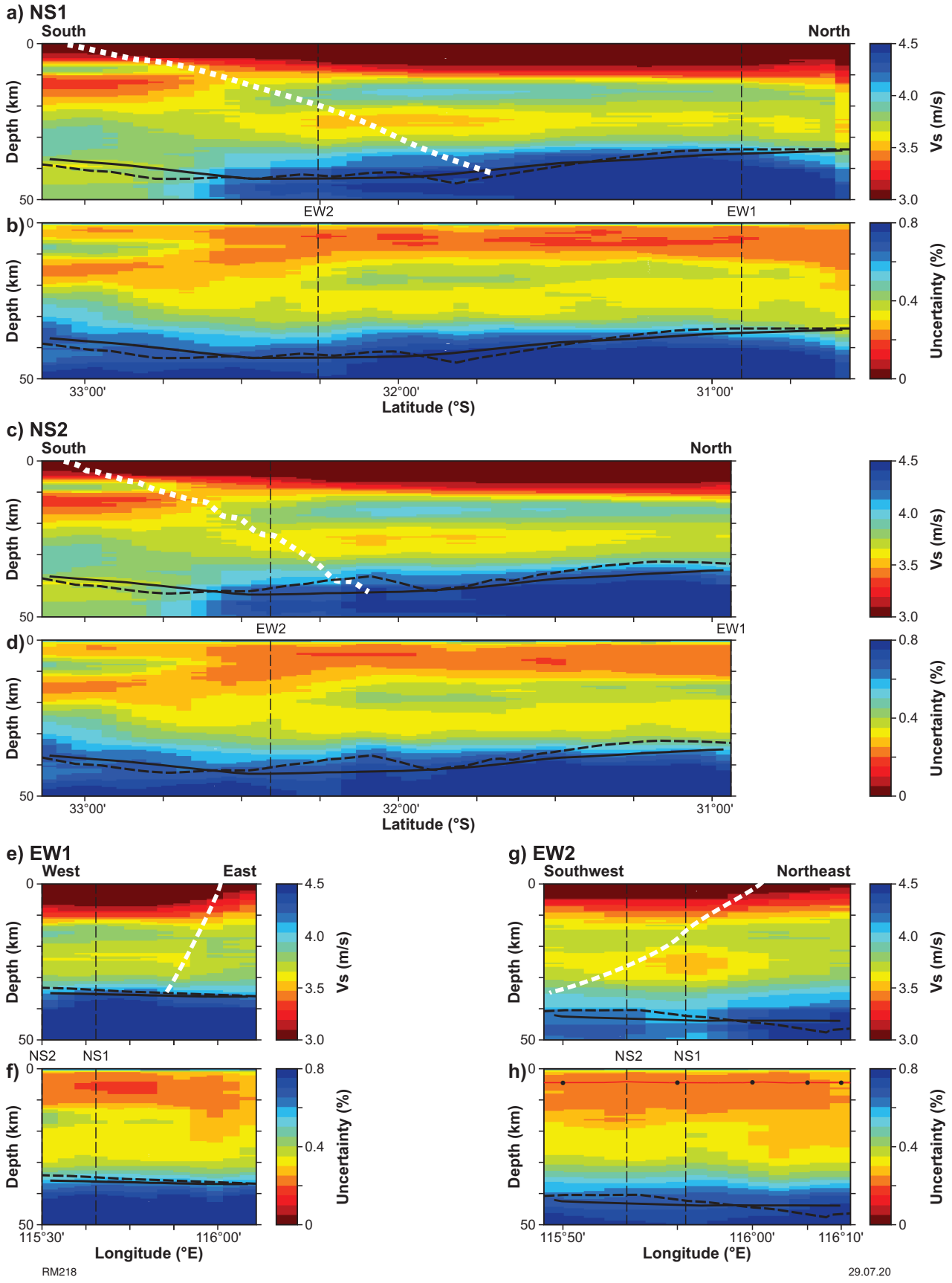

Figure 10. Ambient noise profiles for the Perth Basin transects: a, c, e, g) ambient noise profiles NS1, NS2, EW1, EW2; b, d, f, h) error plots for each ambient noise profile. Solid black line shows the AuSREM Moho and the dashed black line shows the MoGGIE Moho. Note the axis for EW2 is by longitude, but since the profile is oblique to the lines of longitude, the scale does not represent true distance. The location of all profiles can be found in Figure 7

The ambient noise model shows a high-velocity layer appearing at approximately 35–40 km depth. It is seen on all the profiles and is consistent with the AuSREM Moho (Salmon et al., 2012). Looking at the CCP-derived velocity gradients, we would expect to see a strong positive gradient associated with the Moho; however, a negative gradient is seen at the expected depths. Therefore, we suggest that the Moho could be at more than 45 km depth or that the Moho is transitional in this area. Another possibility is that the Moho signal has been obscured by arrivals caused by strong velocity gradients in the shallower part of the section.

A possible Moho-related feature is seen in the CCP images at the extreme north and south of the NS profiles where the errors are lower (Fig. 8b). This, and an equivalent feature seen in profile EW1, leads us to interpret the Moho in this area to occur at about 32–36 km depth. On profile EW1, the Moho signal changes where the profile crosses the Darling Fault Zone.

The lack of a clear Moho underneath the Perth Basin and metropolitan area remains unexplained.

Comparison with gravity modelling

One of the project aims was to image the Moho. The Moho in this area was previously modelled using the AuSREM (Salmon et al., 2012) and Moho geometry gravity inversion experiment (MoGGIE) models (Aitken, 2010). However, both of these models have extrapolated the Moho into this area as there are no local reliable estimates of its depth. Another model was tested that superimposed rough estimates of the Moho from the passive seismic study onto the MoGGIE Moho. All models have a similar shape (Fig. 11), with a deeper Moho under the southern and central Perth Basin. The shallower Moho offshore is an indication of the transition to oceanic crust. Modelling of the isostatic state of the northern Perth Basin showed differences in the crustal structure and effective elastic thickness associated with the different structural elements of the basin (Holzrichter et al., 2014). The area lacks reliable constraints that allow a proper interpretation of Moho depth, which requires the testing of various assumptions on the isostatic state of the area. A model that incorporated modifications to a pre-existing Moho model derived from continent-wide inversion of gravity data could explain the gravity anomalies over the northern Perth Basin (Holzrichter et al., 2014).

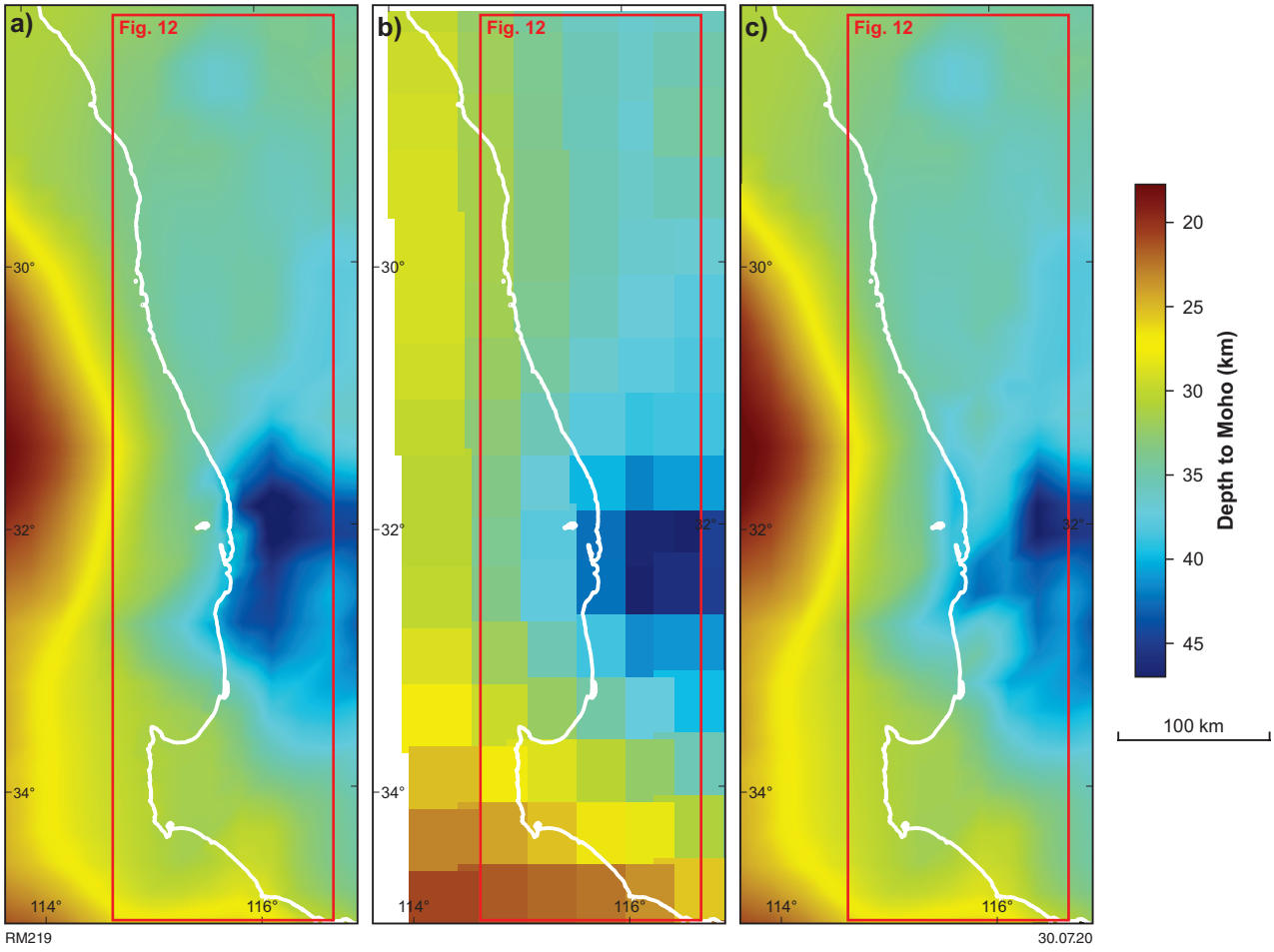

Figure 11. Modelled Moho depths: a) MoGGIE model (Aitken, 2010); b) AuSREM Moho (Salmon et al., 2012); c) depths estimated from the passive seismic study superimposed onto the MoGGIE Moho model. In each map, the area of the forward gravity model (Fig. 12) is shown by the red box

In this study, two basic gravity forward models were created using the MoGGIE Moho (Model 1) and the passive seismic-modified MoGGIE Moho (Model 2). The block models were built in GOCAD (Fig. 12) and forward modelled using VPmg software (Fullagar et al., 2008). They were constructed using the bodies and densities given in Table 1. The model comprised a four-layer Perth Basin taken from the Olierook et al. (2015) model, where the geometries of the basin are constrained by seismic reflection data, the Youanmi and Southwest Terranes of the Yilgarn Craton, the Pinjarra and Albany–Fraser Orogen. The Archean–Proterozoic components were all given very similar densities as they are all predominantly granitic, and the Perth Basin was given densities after Holzrichter et al. (2014) and Olierook et al. (2015). These densities were adjusted to give a better fit to the Bouguer anomaly (Table 1), but otherwise no further adjustments to model geometry were applied.

In both cases, the observed Bouguer anomaly shows a low-gravity response associated with the low-density sediments of the Perth Basin, which is most prominent within the Dandaragan Trough (Fig. 13a; also noted by Holzrichter et al., 2014). The calculated anomaly shows a strong negative anomaly across the whole of the Perth Basin (Fig. 13b) and into the South West Terrane of the Yilgarn Craton. The residual anomaly (Fig. 13c) shows that the model has a mass deficit (positive residual) across the central and southern Perth Basin and over the flanking margin of the Yilgarn Craton. The location of this anomaly is coincident with the deepening of the MoGGIE Moho evident in Figure 11a and in areas farther west.

The apparent shallowing of the Moho by approximately 5 km by using the passive seismic data integrated into the MoGGIE model gave a better fit to the Bouguer anomaly by about 4 mgal (Fig. 13d,e).

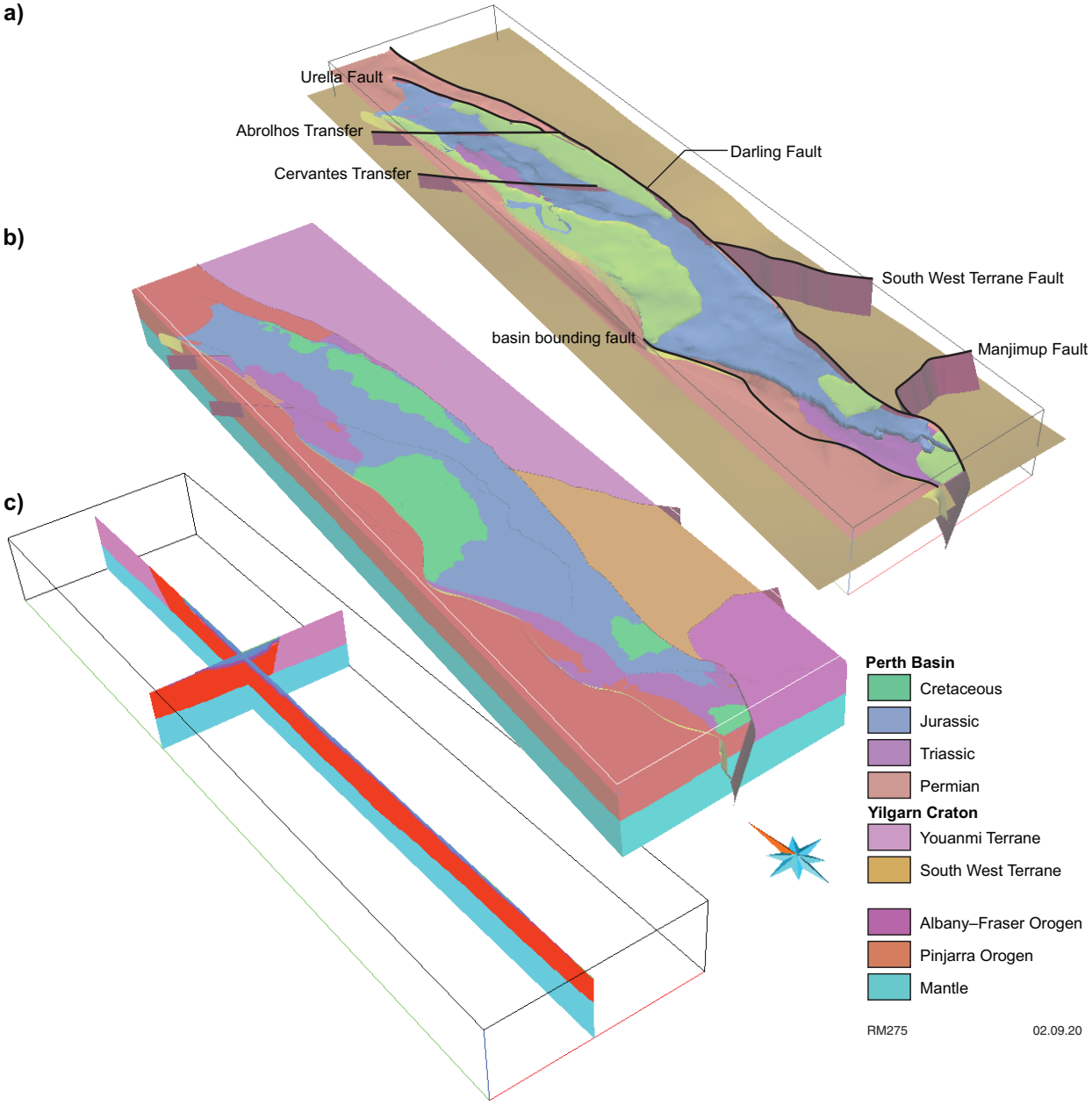

Figure 12. 3D block model of the Perth Basin used in the gravity modelling: a) 3D model with the basement stripped away to show the bounding faults; b) full 3D block model; c) north–south and east–west sections across the block model coloured by lithology

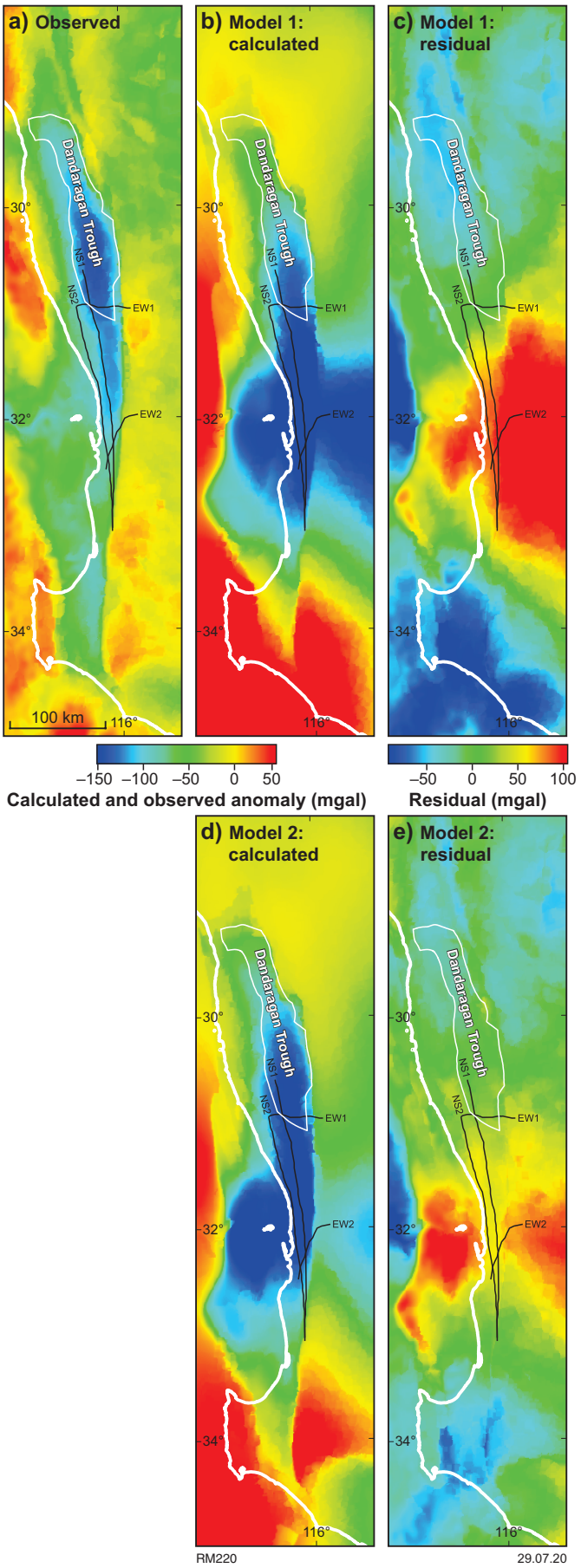

Figure 13. Observed and calculated Bouguer anomalies of the Perth Basin models: a) observed Bouguer anomaly of the Perth Basin model; b) calculated Bouguer anomaly of the forward model for Model 1; c) residual anomaly of the MoGGIE Moho model (Model 1); d) calculated Bouguer anomaly of the forward model (Model 2); e) residual anomaly of the passive seismic Moho integrated with the MoGGIE Moho model (Model 2)

Table 1. Units and densities used in forward gravity modelling of the Perth Basin area for both versions of the model

Unit	*Starting density**	*Adjusted density**
Perth Basin — Cretaceous	–0.4700	–0.4194
Perth Basin — Jurassic	–0.3700	–0.2744
Perth Basin — Triassic	–0.2200	–0.1438
Perth Basin — Permian	–0.0200	0.0256
Pinjarra Orogen	0.1300	0.1281
Albany–Fraser Orogen	0.1300	0.0617
Yilgarn Craton, Youanmi Terrane	0.1300	0.1384
Yilgarn Craton, South West Terrane	0.1400	0.1810
Mantle	0.6300	0.6300

NOTE: * Relative to a background density of 2.67 g/cm^3

However, the uncertainties associated with the picking of the Moho from the passive seismic data are so large and with poor horizontal resolution that this exercise simply shows that variations in the Moho can account for some of the residual anomaly. The residual anomaly is less likely to be caused by uncertainties in the depths of the layers within the Perth Basin, as they are reasonably well constrained from drillholes and seismic reflection surveys. But errors in the estimations of the densities and heterogeneities in the basin sediments or within the basement rocks could all contribute to the difference in observed and calculated gravity anomaly.

Without being able to constrain the geometry of the Moho from the passive seismic methods with more certainty, we are unable to make objective comments on which of the above reasons are most likely to be the cause of the mismatch with the observed gravity anomaly.

Discussion

These seismic data have produced some results of interest, although the main aim of imaging the Moho was not achieved as well as had been hoped and hence no further comment can be made on the opening mechanism for the Perth Basin. Although stations were deployed for up to nine months, the actual recording time was often much shorter due to battery problems. Longer recording times would have resulted in the capture of many more earthquakes and stronger stacked signals, and hence produced better outcomes.

The longer deployments in the Perth metropolitan area (i.e. the central part of the profiles) is reflected in lower errors in those parts of the profiles. However, this proved to be a difficult environment to obtain good results. Nonetheless, the data recorded within the Perth metropolitan area show that recording useful data is possible within such noisy environments if a long enough deployment period is used.

Data quality was also affected by the mix of sensitivities of the instruments, with approximately half the seismometers having a 120 s – 100 Hz period range and the other half having a 20 s – 100 Hz period range. Burying the seismometers might also have resulted in improvements in data quality.

Summary

The passive seismic experiment shows the Perth Basin to be around 10 km thick in the study area. The basement to the basin appears to have a consistent velocity structure with the exception of a region between 31.5 and 32.3°S, where a different velocity structure may indicate a geologically distinct component of the Pinjarra Orogen. The Moho in the region is poorly constrained by the data due to poor signal-to-noise levels, but is probably at more than 45 km depth and may be represented by a velocity transition rather than a sharp discontinuity.

Acknowledgements

Our thanks go to the ANSIR for the loan of equipment, and the Pawsey Centre for use of supercomputing facilities. Many thanks go to the landowners who allowed us to install a seismometer on their properties.

References

Aitken, ARA 2010, Moho geometry gravity inversion experiment (MoGGIE): A refined model of the Australian Moho, and its tectonic and isostatic implications: Earth and Planetary Science Letters, v. 297, p. 71–83.

Ammon, CJ 1991, The isolation of receiver effects from teleseismic P waveforms: Bulletin of the Seismological Society of America, v. 81, no. 6, p. 2504–2510.

Bensen, GD, Ritzwoller, MH, Barmin, MP, Levshin, AL, Lin, F, Moschetti, MP, Shapiro, NM and Yang, Y 2007, Processing seismic ambient noise data to obtain reliable broad-band surface wave dispersion measurements: Geophysical Journal International, v. 169, no. 3, p. 1239–1260.

Byrne, DR and Harris, LB 1992, Fault patterns during normal and oblique rifting and the influence of basement discontinuities: Application to models for the Perth Basin, Western Australia, *in* Ninth International Conference on Basement Tectonics, Canberra, Australia, 1990/07 *edited by* MJ Rickard, HJ Harrington and PR Williams: Springer (Basement Tectonics 9), p. 23–42.

Cockbain, AE and Lehmann, PR 1971, Geology of the Perth Basin, Western Australia. Part 1 — Regional stratigraphy and structure; Ashburton Oil N.L.: Geological Survey of Western Australia, Statutory petroleum exploration report W1129, 31p (unpublished).

Crostella, A 1995, An evaluation of the hydrocarbon potential of the onshore northern Perth Basin, Western Australia: Geological Survey of Western Australia, Report 43, 67p.

Crostella, A and Backhouse, J 2000, Geology and petroleum exploration of the central and southern Perth Basin, Western Australia: Geological Survey of Western Australia, Report 57, 85p.

Delle Piane, C, Esteban, L, Timms, NE and Ramesh, I 2013, Physical properties of Mesozoic sedimentary rocks from the Perth Basin, Western Australia: Australian Journal of Earth Sciences, v. 60, no. 6–7, p. 735–745.

Dentith, MC, Bruner, I, Long, A, Middleton, MF and Scott, J 1993, Structure of the Eastern Margin of the Perth Basin, Western Australia: Exploration Geophysics, v. 24, no. 3–4, p. 455–461.

Dentith, MC, Long, A, Scott, J, Harris, LB and Wilde, SA 1994, The influence of basement on faulting within the Perth Basin, Western Australia, *in* The sedimentary basins of Western Australia: Proceedings of the West Australian Basins Symposium, Perth, Western Australia, 14–17 August 1994 *edited by* PG Purcell and RR Purcell: Petroleum Exploration Society of Australia, p. 791–799.

Dueker, KG and Sheehan, AF 1997, Mantle discontinuity structure from midpoint stacks of converted P to S waves across the Yellowstone hotspot track: Journal of Geophysical Research, v. 102, B4, p. 8313–8327.

Efron, B and Tibshitani, R 1986, Bootstrap methods for standard errors, confidence intervals, and other measures of statistical accuracy: Statistical Science, v. 1, p. 54–77.

Fletcher, IR and Libby, WG 1993, Further isotopic evidence for the existence of two distinct terranes in the southern Pinjarra Orogen, Western Australia, *in* Professional papers: Geological Survey of Western Australia: Report 34, p. 81–84.

Fullagar, PK, Pears, GA and McMonnies, B 2008, Constrained inversion of geologic surfaces — pushing the boundaries: The Leading Edge, v. 27, no. 1, p. 98–105.

Gibbons, AD, Barckhausen, U, den Bogaard, P, Hoernle, K, Werner, R, Whittaker, JM and Müller, RD 2012, Constraining the Jurassic extent of Greater India: Tectonic evolution of the West Australian margin: Geochemistry, Geophysics, Geosystems, v. 13, no. 5, p. 1–25.

Green, PF and Duddy, IR 2013, The influence of exhumation on petroleum prospectivity in the sedimentary basins of WA, *in* The sedimentary basins of Western Australia: Proceedings of the West Australian Basins Symposium *edited by* M Keep and SJ Moss: West Australian Basins Symposium, Perth, Western Australia, 18–21 August 2013: Petroleum Exploration Society of Australia, A1–A15.

Haig, DW, McCartain, E, Mory, AJ, Borges, G, Davydov, VI, Dixon, M, Ernst, A, Groflin, S, Håjabssib, E, Keep, M, Dos Santos, Z, Shi, GR and Soares, J 2014, Postglacial Early Permian (Sakmarian-Artinskian) shallow-marine carbonate deposition along a 2000 km transect from Timor to west Australia: Palaeogeography, Palaeoclimatology, Palaeoecology, v. 409, p. 180–204.

Hall, L, Hackney, R and Johnston, S 2012, Understanding Australia's Southwest Margin: Basement architecture as a framework for predictive basin analysis: AusGeo News, v. 105, p. 3–9.

Harris, LB 1994, Structural and tectonic synthesis of the Perth Basin, Western Australia: Journal of Petroleum Geology, v. 17, p. 129–156.

Hocking, RM 1991, The Silurian Tumblagooda Sandstone, Western Australia: Geological Survey of Western Australia, Report 27, 124p.

Holzrichter, N, Hackney, R and Johnston, S 2014, Crustal structure of the northern Perth Basin, southwest margin of Australia: insights from three-dimensional density models: Geophysical Journal International, v. 196, no. 1, p. 204–217.

Hoskin, TE 2017, Assessment of the North Perth Basin for geothermal resources using integrated geophysical approach; The University of Western Australia, Australia, PhD thesis (unpublished), 257p.

Iasky, RP 1993, A structural study of the southern Perth Basin, Western Australia: Geological Survey of Western Australia, Report 31, 56p.

Iasky, RP and Lockwood, AM 2004, Gravity and magnetic interpretation of the southern Perth Basin, Western Australia: Geological Survey of Western Australia, Record 2004/8, 32p.

Iasky, RP and Shevchenko, SI 1996, Onshore northern Perth Basin gravity project: Geological Survey of Western Australia, Record 1995/6, 21p.

Janssen, DP, Collins, AS and Fitzsimons, ICW 2003, Structure and tectonics of the Leeuwin Complex and Darling Fault Zone, southern Pinjarra Orogen, Western Australia — a field guide: Geological Survey of Western Australia, Record 2003/15, 33p.

Johnson, SP 2013, The birth of supercontinents and the Proterozoic assembly of Western Australia: Geological Survey of Western Australia, 78p.

Jones, AT, Kennard, JM, Nicholson, CJ, Bernardel, G, Mantle, D, Grosjean, E, Boreham, CJ, Jorgensen, DC and Robertson, D 2011, New exploration opportunities in the offshore northern Perth Basin: The APPEA Journal, p. 45–78.

Jones, DK and Pearson, GR 1972, The tectonic elements of the Perth Basin: The APEA Journal, v. 12, no. 1, p. 17–22.

Kuuskraa, V, Stevens, S, van Leeuwen, T and Moodhe, K 2011, Australia, *in* World shale gas resources: an initial assessment of 14 regions outside the United States — a report prepared for U.S. Energy Information Administration at the U.S. Department of Energy: Advanced Resources International Inc, Arlington, Virginia, US, XIV-1–XIV-27.

Kuuskraa, V, Stevens, S, van Leeuwen, T and Moodhe, K 2013, Australia, *in* Technically Recoverable Shale Oil and Shale Gas Resources: An Assessment of 137 Shale Formations in 41 Countries Outside the United States - a report prepared for U.S. Energy Information Administration at the U.S. Department of Energy: Advanced Resources International Inc, Arlington, Virginia, US, III-1–III-49.

Levshin, AL, Pisarenko, VF and Pogrebinsky, GA 1972, On a frequency time analysis of oscillations: Annales Geophysicae, v. 28, no. 2, p. 211–218.

Lowry, DC 1965, Geology of the Southern Perth Basin: Geological Survey of Western Australia, Record 1965/17, 62p.

Markwitz, V, Kirkland, CL, Wyrwoll, K-H, Hancock, EA, Evans, NJ and Lu, Y 2017, Variations in zircon provenance constrain age and geometry of an early Paleozoic rift in the Pinjarra Orogen, East Gondwana: Tectonics, v. 36, p. 2477–2496.

Middleton, M 2016, Radiogenic heat generation in Western Australia — Implications for geothermal energy, *in* Advances in geothermal energy *edited by* BI Ismail: Intech, p. 49–90.

Middleton, MF, Long, A, Wilde, SA, Dentith, M and Evans, BA 1993, A Preliminary Interpretation of Deep Seismic Reflection and other Geophysical Data from the Darling Fault Zone, Western Australia: Exploration Geophysics, v. 24, no. 3–4, p. 711–717.

Millar, AS and Reeve, JS 2014, GSWA Harvey 1 well completion and preliminary interpretation report, southern Perth Basin: Geological Survey of Western Australia, Record 2014/12, 17p.

Mory, AJ and Hocking, RM 2008, Geology of the Kalbarri and Mingenew areas — a field guide: Geological Survey of Western Australia, Record 2008/11, 34p.

Mory, AJ and Iasky, RP 1996, Stratigraphy and structure of the onshore northern Perth Basin, Western Australia: Geological Survey of Western Australia, Report 46, 101p.

Nicholson, CJ, Borissova, I, Krassay, AA, Boreham, CJ, Monteil, E, Neumann, V, Di Primio, R and Bradshaw, BE 2008, New exploration opportunities in the southern Vlaming Sub-basin: APPEA Journal, v. 2008, p. 371–380.

Norvick, MS 2004, Tectonic and stratigraphic history of the Perth Basin: Geoscience Australia, Record 2004/16, 30p.

Olierook, HKH, Timms, NE, Wellmann, JF, Corbel, S and Wilkes, PG 2015, 3D structural and stratigraphic model of the Perth Basin, Western Australia: Implications for sub-basin evolution: Australian Journal of Earth Sciences, v. 62, no. 4, p. 447–467, doi:10.1080/08120099.2015.1054882.

Olierook, HKH, Jourdan, RE, Timms, NE, Kusznir, N and Muhling, JR 2016, Bunbury Basalt: Gondwana breakup products or earliest vestiges of the Kerguelen mantle plume? Earth and Planetary Science Letters, v. 440, p. 20–32.

Playford, PE 1971, Petroleum exploration in Western Australia, past, present, and future: Royal Society of Western Australia Journal, v. 54, p. 1–13.

Playford, PE, Cockbain, AE and Low, GH 1976, Geology of the Perth Basin, Western Australia: Geological Survey of Western Australia, Bulletin 124, 311p.

Playford, PE, Cope, RN, Cockbain, AE, Low, GH and Lowry, DC 1975, Canning Basin, *in* The geology of Western Australia: Geological Survey of Western Australia: Memoir 2, p. 319–368.

Pujol, M, Ricard, LP and Bolton, G 2015, 20 years of exploitation of the Yarragadee aquifer in the Perth Basin of Western Australia for direct use of geothermal heat: Geothermics, v. 57, p. 39–55.

Quaife, R, Rosser, J and Pagnozzi, S 1994, The structural architecture and stratigraphy of the offshore northern Perth Basin, Western Australia, *in* The sedimentary basins of Western Australia: Proceedings of the West Australian Basins Symposium, Perth, Western Australia, 14–17 August 1994 *edited by* PG Purcell and RR Purcell: Petroleum Exploration Society of Australia, p. 811–822.

Rawlinson, N and Sambridge, M 2005, The fast marching method: an effective tool for tomographic imaging and tracking multiple phases in complex layered media: Exploration Geophysics, v. 36, no. 4, p. 341–350.

Salmon, M, Kennett, BLN and Saygin, E 2012, Australian Seismological Reference Model (AuSREM): Crustal component: Geophysical Journal International, v. 192, p. 190–206.

Saygin, E and Kennett, BLN 2010, Ambient noise tomography for the Australian Continent: Tectonophysics, v. 481, p. 116–125.

Saygin, E and Kennett, BLN 2012, Crustal structure of Australia from ambient seismic noise tomography: Journal of Geophysical Research: Solid Earth, v. 117, B01304, 15p.

Sealy, BE 1969, Harvey (239) Seismic Project, Final Report, Perth Basin: Geological Survey of Western Australia, Statutory petroleum exploration report S471 A3, 64p (unpublished).

Shapiro, NM and Campillo, M 2004, Emergence of broadband Rayleigh waves from correlations of the ambient seismic noise: Geophysical Research Letters, v. 31, no. 7, p. 1–4.

Shragge, J, Yang, J, Issa, NA, Roelens, M, Dentith, M and Schediwy, S 2019, Low-frequency ambient Distributed Acoustic Sensing (DAS): Useful for subsurface investigation?: Society of Exploration Geophysicists Annual Meeting, 89th Meeting, p. 963–967, doi:10.1190/segam2019-3216479.1.

Song, T and Cawood, PA 2000, Structural styles in the Perth Basin associated with break-up of Greater India and Australia: Tectonophysics, v. 317, p. 55–72.

Symonds, PA and Cameron, PJ 1977, The structure and stratigraphy of the Carnarvon Terrace and Wallaby Plateau: The APEA Journal, v. 17, p. 30–41.

Thomas, CM 2014, The tectonic framework of the Perth Basin: Current understanding: Geological Survey of Western Australia, Record 2014/14, 36p.

Thomas, CM 2018, Regional seismic interpretation and structure of the southern Perth Basin: Geological Survey of Western Australia, Report 184, 52p.

Timms, N, Wilkes, P, Corbel, S, Horowitz, F and Healy, D 2012, Revealing faults in the Perth metropolitan area, Western Australia: implications for ground water systematics, *in* Proceedings of the 34th International Geological Congress, Brisbane Queensland, 5–10 August 2012: Australian Geosciences Council.

Thyer, RF and Everingham, IB 1956, Gravity survey of the Perth Basin, Western Australia: Bureau of Mineral Resources, Geology and Geophysics, Bulletin 33, 20p.

Tupper, NP, Phillips, SE and Williams, BPJ 1994, Advances in the understanding of Upper Permian reservoir distribution and quality, north Perth Basin, *in* The sedimentary basins of Western Australia: Proceedings of the West Australian Basins Symposium, Perth, Western Australia, 14–17 August 1994 *edited by* PG Purcell and RR Purcell: Petroleum Exploration Society of Australia, p. 823–837.

Wilde, SA 1999, Evolution of the western margin of Australia during the Rodinian and Gondwanan supercontinent cycles: Gondwana Research, v. 2, p. 481–499.

Yuan, H and Bodin, T 2018, A probabilistic shear wave-velocity model of the crust in the central West Australian Craton constrained by transdimensional inversion of ambient noise dispersion: Tectonics, v. 37, no. 7, p. 1994–2012.

Zhan, Y 2014, 2D seismic interpretation of the Harvey area, southern Perth Basin, Western Australia: Geological Survey of Western Australia, Record 2014/7, 25p.

Murdie et al.

A PASSIVE SEISMIC EXPERIMENT IN THE PERTH BASIN, WESTERN AUSTRALIA

This Report presents the results of a study attempting to image the Moho underneath the Perth Basin in order to gain insights into the mechanism of its formation by using passive seismic techniques. The experiment shows the Perth Basin to be around 10 km thick in the study area and appears to have a consistent velocity structure with the exception of a region between 31.5 and 32.3°S where a different velocity structure may be indicative of a geologically distinct component of the Pinjarra Orogen.

Further details of geoscience products are available from:

Information Centre
Department of Mines, Industry Regulation and Safety
100 Plain Street
EAST PERTH WA 6004
Phone: (08) 9222 3459 Email: publications@dmirs.wa.gov.au

www.dmirs.wa.gov.au/GSWApublications

REPORT 208